Image processing methods to obtain symmetrical distribution from projection image

Asano, Hitoshi ; Takenaka, Nobuyuki ; Fujii, Terushige ; Nakamatsu, E ; Tagami, Y ; Takeshima, K

Image Processing Methods to Obtain Symmetrical Distribution from Projection Image

H. ASANO[*1], N. TAKENAKA[*1], T. FUJII[*1], E. NAKAMATSU[*1], Y. TAGAMI[*1], K. TAKESHIMA[*2]

*1 Department of Mechanical Engineering, Kobe University

1-1, Rokkodai-cho, Nada-ku, Kobe 657-8501, Japan

Fax : +81-78-803-6122, E-mail : asano@mech.kobe-u.ac.jp

*2 Department of Mechanical Engineering, Kochi National College of Technology

200-1, Monobe, Nankoku, Kochi 783-8508, Japan

Abstract

Flow visualization and measurement of cross-sectional liquid distribution is a very effective tool to clarify the effects of obstacles in a conduit on heat transfer and flow characteristics of gas-liquid two-phase flow. In this study, two methods to obtain cross-sectional distribution of void fraction are applied to vertical upward air-water two-phase flow. These methods need projection images from only one direction. Radial distributions of void fraction in a circular tube and a circular-tube annuli with a spacer were calculated by the Abel transform based on the assumption of axial symmetry. On the other hand, cross-sectional distributions of void fraction in a circular tube with a wire coil whose conduit configuration rotates about the tube central axis periodically were measured by the CT method based on the assumption that the relative distribution of liquid phase against the wire was kept along the flow direction.

Keywords: Neutron radiography, Gas-liquid two-phase flow, Cross-sectional void fraction distribution, CT method, Abel transform

1. Introduction

Obstacles are often placed in a conduit for heat transfer enhancement or as fixing tool in tube banks. In the case where the working fluids flow as a gas-liquid two-phase mixture, heat transfer and flow characteristics are strongly influenced by phase distribution. Obstacles also influence phase distribution. It is important for the design to clarify the phase distribution in this kind of equipment.

Neutron radiography is an efficient tool for visualization of gas-liquid two-phase flow, since that equipment is usually made by metallic material. Information obtained by neutron radiography is integrated along the beam direction. Therefore, other information from various directions or an assumption on phase distribution is necessary to estimate cross-sectional distributions. If some projection images from several directions could be obtained under the same condition, a cross-sectional distribution of void fraction can be measured by CT reconstruction. For void fraction measurement, at least two kinds of projection images, i.e., only the test section and the test section with gas-liquid two-phase flow, are needed. Therefore, it takes a long time for void fraction measurement by a CT method. This is not desirable from the standpoint of the radio activation of an object and maintenance of flow condition.

In this study, two calculating methods, by which cross-sectional void fraction distribution can be calculated based on an assumption of phase distribution, were applied to images visualized by thermal neutron radiography. One is the case where both cross-section of conduit and phase distribution are rotated about the central axis simultaneously. This case is often seen in enhanced heat transfer tubes. Another one is the case where the phase distribution has axial symmetry. Image processing methods and processed results on cross-sectional distributions of void fraction are reported in this paper.

2. Experimental apparatus and methods

Flow visualization experiments were carried out by utilizing the JRR-3M thermal neutron

radiography facility at JAERI (Japan Atomic Energy Research Institute). A cooled CCD camera was used for high-resolution measurements. Still images consisting of 1000 × 1018 image elements were photographed with an exposure time of four seconds, and were digitized with 14 bit intensity levels.

A schematic diagram of the experimental apparatus for air-water two-phase flow is shown in Fig. 1. Air was fed to a mixing section ***4*** from an air compressor through a pressure regulating valve ***3*** and a gas flow meter. Tap water in a tank ***1***, was fed by a pump ***2*** to the mixing section ***3*** through a water flow meter. The two-phase flow formed in the mixing section flew into a vertical tube in the irradiation room. Three kinds of tubes shown in Figs. (a) and (b) were used as the test section. Fig. 2(a) shows an aluminum circular tube of 16 mm inner diameter and 1 mm thickness with a stainless steel wire coil of 2 mm on the inner wall. The pitch of the coil was 32 mm and the helix angle was 56.9 degree. The second one was an aluminum circular tube of 10 mm inner diameter and 1 mm thickness. The third one shown in Fig. 2(b) was a circular tube annuli with a spacer. An aluminum rod of 10 mm diameter was installed at the central axis of an aluminum circular tube of 20 mm inner diameter with a circular spacer. The spacer was a stainless cylinder of 12 mm inner diameter and 0.5 mm thickness, and was fixed by six pins shown in Fig. 2(b). The clearance between the rod and the spacer was 1 mm.

The experimental conditions were the liquid volumetric fluxes j_L of 0.102 and 0.051 m/s, and the gas volumetric fluxes j_G of 2.0 to 61.8 m/s for a circular tube with a wire coil. On the other hand, j_G and j_L for a circular and circular annuli were in the range of 0.5 to 26 m/s, and 0.02 to 0.4 m/s, respectively. Volumetric flux is defined by the following equation:

$$j_L = Q_L/A, \quad j_G = Q_G/A \tag{1}$$

where Q is volumetric flowrate [m^3/s], and A is cross-sectional area of conduit [m^2].

3. Image processing for void fraction

Assuming the brightness of visualized image is proportional to the beam intensity on a scintillation converter and neglecting the attenuation due to gas phase, a brightness of two-phase flow image $S_{tp}(x,y)$, an image without liquid $S_1(x, y)$, i.e., $\alpha(x, y)=1$, and an image full of liquid $S_0(x, y)$, i.e., $\alpha(x, y)=0$, is expressed as the following equations:

$$S_{tp}(x,y) = G(x,y)\exp\left[-\rho_w\mu_{mw}t_w(x,y) - \{1-\alpha(x,y)\}\rho_L\mu_{mL}t(x,y)\right] + O_{tp}(x,y) \tag{2}$$

$$S_1(x,y) = G(x,y)\exp\left[-\rho_w\mu_{mw}t_w(x,y)\right] + O_1(x,y) \tag{3}$$

$$S_0(x,y) = G(x,y)\exp\left[-\rho_w\mu_{mw}t_w(x,y) - \rho_L\mu_{mL}t(x,y)\right] + O_0(x,y) \tag{4}$$

where subscripts of w and L mean the wall and the liquid, respectively, and $t(x, y)$ means the thickness of the two-phase flow area at coordinate (x, y). $\alpha(x, y)$ is the averaged void fraction along the neutron beam. $G(x, y)$ is the gain and it depends on the position due to the non-flatness of initial beam intensity and of sensitivity in an imaging system. $O(x, y)$ is the offset. The variations of brightness caused by neutron scattering in an object and optical scattering in a neutron camera were considered in the offset value, that is, the offset is due to the dark current, the neutron scattering, and the optical scattering. The offset value depends on the flow pattern. To measure void fraction quantitatively, it is necessary to estimate the offset value under each experimental condition.

Using Eqs. (1) to (3) , two-dimensional distribution of liquid thickness along the beam direction can be expressed as

$$(1-\alpha(x,y))t(x,y) = \frac{1}{\rho_L\mu_{mL}}\ln\left\{\left[S_1(x,y)-O_1(x,y)\right]/\left[S_{tp}(x,y)-O_{tp}(x,y)\right]\right\} \tag{5}$$

In the case that conduit configuration rotates about the tube central axis periodically, a CT method can be applied to a 2D projected distribution of liquid thickness based on the assumption that relative cross-sectional liquid distributions to a wire coil are kept along flow direction. This method was applied to a gas-liquid two-phase flow in a circular-tube with a wire coil.

On the other hand, assuming that a cross-sectional distribution of void fraction is axial symmetry, the radial distribution of void fraction can be calculated by Abel transform on projected data from one direction. Chord integrals of void fraction as illustrated in Fig.3 are formularized by the following equation:

$$I(x,y) = t(x,y)\alpha(x,y) = \int_{(x,y)line} \alpha(r,y)dz \tag{6}$$

where $t(x, y)$ means the thickness of two-phase flow area, $\alpha(x, y)$ is the average value along beam direction, and $\alpha(r, y)$ is the local value at radius of r. We may change the z integral into an r integral by the Abel transform to get

$$I(x,y) = 2\int_{r}^{r_w} \alpha(r,y)\frac{rdr}{\sqrt{r^2 - x^2}} \tag{7}$$

Performing inverse transformation,

$$\alpha(r,y) = \frac{1}{\pi}\int_{r}^{r_w} \frac{dI(x,y)}{dx}\frac{dx}{\sqrt{x^2 - r^2}} \tag{8}$$

Since calculated results of $I(x, y)$ are discrete data, Eq. (8) is solved by Simpson formula as follows;

$$\alpha(r,y) = \frac{\delta}{3}\left[g(r,y) + 4\sum_{i=1}^{m} g(r + (2i-1)\delta, y) + 2\sum_{i=1}^{m-1} g(r + 2m\delta, y) + g(r_w, y) \right] \tag{9}$$

$$g(x,y) = \frac{dI(x,y)}{dx}\frac{1}{\sqrt{x^2 - r^2}} \tag{10}$$

where δ is width of a pixel, i.e., $\delta = x_m - x_{m-1}$.

The central difference is applied to the derivative of $I(x, y)$ with respect to x. $\alpha(r, y)$ can be calculated from the measured results of $I(x, y)$ by using equations (8) to (10).

4. Results and discussion

4.1 Gas-liquid two-phase flow in a circular tube with a wire coil

Fig.4 shows visualized results of the tube with the wire coil photographed by the cooled CCD camera. There are many distributed white spot noises in the original image. These figures are the images after removing the noise by a morphological filter (Motomura, et al., 1997). In the image of only the test section (Fig. 4(a)), the stainless wire coil was clearly visualized. Fig. 4(b) show the images with gas-liquid two-phase flow. Gas volumetric flux was varied 2.0, 10.3, and 61.8 m/s with a constant j_L of 0.102 m/s. The brightness of image in the flow region increased with increasing of j_G. The void fraction may become higher with j_G. Liquid phase just downstream of the wire looks larger than that upstream of the wire.

One-dimensional distributions of cross-sectional averaged void fraction are plotted in Fig. 5 against the distance from the gas-liquid mixing section. That in a circular tube with the same inner diameter of 16 mm is also plotted. The values of j_G and j_L were the highest in this experimental range. It can be seen that void fractions are almost constant in the visualized area in each tube. The gas-liquid two-phase flow was fully developed in the visualized range. A CT method was applied to liquid thickness distributions calculated by Eq.(5) from projection image. An example of liquid thickness distribution is shown in Fig. 6. This image was used as a sinogram in a CT method. The length of the object is equal to the half of the pitch of the wire coil, i.e., 16 mm, and the image consists of 78 pixels. That is to say, this image is equivalent to 78 projections rotating half rotation with an interval of 2.34 degrees.

Calculated results of cross-sectional distribution of void fraction are shown in Fig. 7. The values were shown by a gray scale in arbitrary unit. Black rings show liquid on the inner wall. The small white oval at the left side in the black ring shows the wire. The area upside and downside of the white oval is equivalent to the upstream and downstream of the wire, respectively. That is to say, counter clockwise rotation is equivalent to the flow direction. At low gas velocity with j_G=2.0 m/s, the black area near the wall was large, and the difference between the upstream and the downstream of the wire coil was small. The reason is estimated that the flow pattern was an intermittent or a churn flow, and the liquid thickness on the wall was larger than the wire diameter. On the other hand, increasing j_G, liquid fraction became lower and the difference across the wire became larger. The liquid fraction at the upstream of the wire was lower than that at the downstream. The liquid phase may be stagnant in a wake of the wire due to gravity and weak gas velocity. The same tendency is seen in Fig. 7(b) under lower liquid volumetric flux, j_L=0.05 m/s.

4.2 Gas-liquid two-phase flow in circular-tube and circular-tube annuli with a spacer

Visualized images of a vertical circular-tube are shown in Fig. 8. A B_4C grid was placed in the front of the test section for quantitative measurements by the umbra method (Takenaka, et al., 2001). The width and interval of the B_4C grid are both 3 mm. In Fig. 8 (b), (i), the stainless steel spacer is clearly visualized. Brightness distributions of images with gas-liquid two-phase flow were bilateral symmetry for the both tubes. Void fraction distributions may be axial symmetry.

Fig. 9 shows the axial distribution of cross-sectional averaged void fraction in the circular-tube annuli. Quantitatively calculated results are plotted for values of j_G from 0.77 to 25.7 m/s and a constant j_L of 0.12 m/s. For higher gas volumetric flux (j_G < 15 m/s), the effect of the spacer on $\overline{\alpha}$ was small. However, in the range of j_G < 15 m/s, the effect became larger, i.e., decreased rapidly at the

inlet of the spacer, increased gradually in the spacer, and recovered rapidly at the exit.

Radial distributions of void fraction calculated by using the Abel transform are plotted in Fig. 10 for different spatial resolution. Spatial resolution was changed by the lens of CCD camera. The effect of spatial resolution was small.

Radial void fraction distributions in circular-tube and circular-tube annuli with a spacer are shown in Figs.11 (a) to (c). The effect of j_G was small for the circular-tube and the circular-tube annuli. On the other hand, void fraction in a space between the inner wall and the spacer decreased in the range of j_G < 15 m/s. The reason for the decrease of $\overline{\alpha}$ in this region with the spacer is found from the calculated results of radial void fraction distributions.

5. Conclusions

Two measuring methods, by which cross-sectional distribution of void fraction can be obtained from projection image from only one direction obtained by neutron radiography, were proposed and applied to vertical upward air-water two-phase flow in a circular-tube, a circular-tube with a wire coil, and a circular-tube annuli with a circular spacer. In the case that configuration of the conduit is rotating about the central axis, assuming that flow is developed and cross-sectional phase distribution is also rotating with the conduit, void fraction distribution can be obtained by a CT method directly using a projection image as a sinogram. On the other hand, in case that phase distribution is expected to be axial symmetry, radial distribution of void fraction can be calculated by Abel transform.

References

Motomura, Y., Ono, A., Yoshii, K., Sonoda, K., 1997, Application of Morphological Filters to noise suppression in Neutron Radiography Image., in “5th World Conf. on Neutron Radiography”, Deutshe Gesellschaft für Zerstörungsfreie Prüfung e.V., pp. 229-236.

Takenaka, N., Asano, H., Fujii, T., Matsubayashi, M., 2001, A Method for Quantitative Measurement by Thermal Neutron Radiography., Nondestructive Testing and Evaluation, 16, pp. 345-354.

List of figures

Fig. 1 Schematic diagram of experimental apparatus.

Fig. 2 Test section configuration.

Fig. 3 Projection of neutron beam (Top view).

Fig. 4 Visualized image of a circular-tube with a wire coil after reducing white spot noises by a morphological filter.

(a) Only the test section.

(b) With gas-liquid two-phase flow.

(i) j_G=2.0 m/s. (ii) j_G =10.3 m/s. (iii) j_G =61.8 m/s

Fig. 5 Axial distribution of cross-sectional averaged void fraction

Fig. 6 Example of sinogram.

Fig. 7 Cross-sectional distribution of liquid fraction in arbitrary unit.

Fig. 8 Visualized image after reducing white spot noises by a morphological filter

(a) Circular-tube.

(b) Circular-tube annuli with a spacer.

Fig. 9 Axial distribution of cross-sectional averaged void fraction in circular-tube annuli.

Fig. 10 Radial distribution of void fraction calculated by Abel transform (Effect of spatial resolution).

Fig. 11 Radial distribution of void fraction calculated by Abel transform.

(a) Circular-tube.

(b) Circular-tube annuli.

(c) Circular-tube annuli with a spacer.

"Image Processing Methods to Obtain Symmetrical Distribution from Projection Image"

H. ASANO, N. TAKENAKA, T. FUJII, E. NAKAMATSU, Y. TAGAMI, K. TAKESHIMA

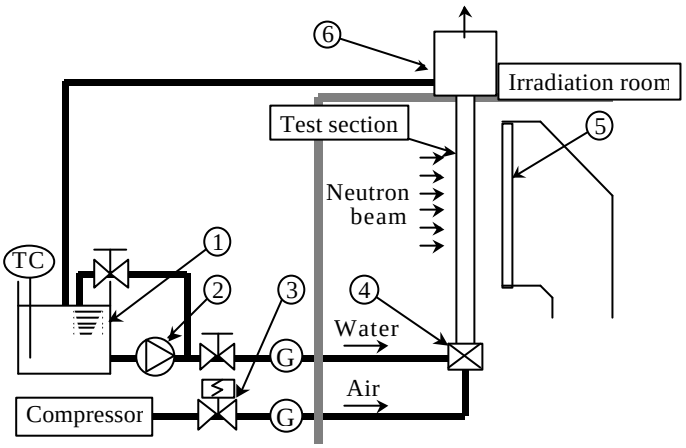

1. Tank
2. Pump
3. Regulating valve
4. Mixing section
5. Scintillation converter
6. Gas/liquid separator
G Flow meter
TC Thermocouple

Fig. 1 Schematic diagram of experimental apparatus.

"Image Processing Methods to Obtain Symmetrical Distribution from Projection Image"

H. ASANO, N. TAKENAKA, T. FUJII, E. NAKAMATSU, Y. TAGAMI, K. TAKESHIMA

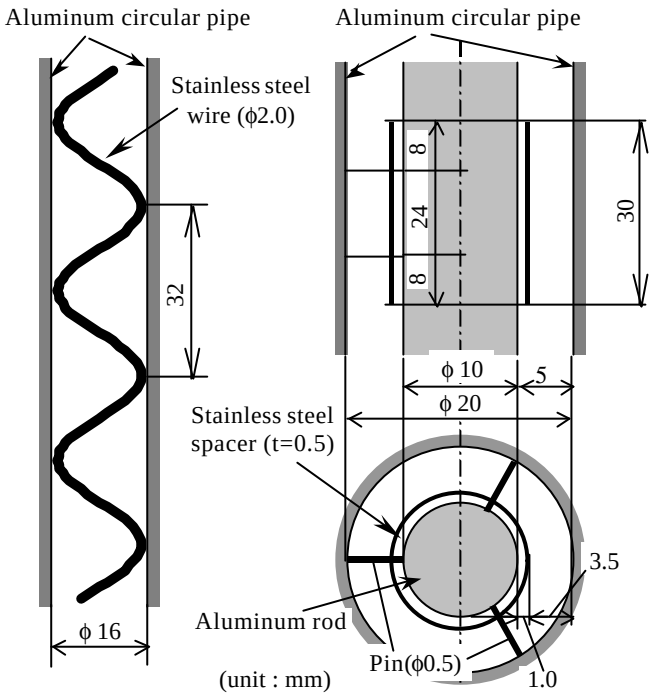

(a) Circular-tube with a wire coil.

(b) Circular-tube annuli with a circular spacer.

Fig. 2 Test section configuration.

“Image Processing Methods to Obtain Symmetrical Distribution from Projection Image”

H. ASANO, N. TAKENAKA, T. FUJII, E. NAKAMATSU, Y. TAGAMI, K. TAKESHIMA

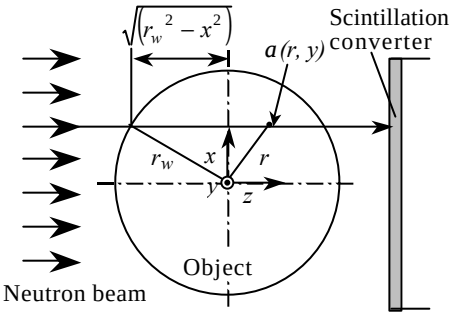

Fig. 3 Projection of neutron beam (Top view).

"Image Processing Methods to Obtain Symmetrical Distribution from Projection Image"

H. ASANO, N. TAKENAKA, T. FUJII, E. NAKAMATSU, Y. TAGAMI, K. TAKESHIMA

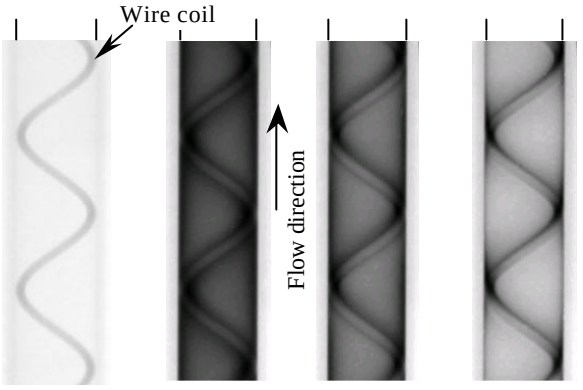

(a) Only test section. (i) j_G=2.0 m/s (ii) j_G=10.3m/s (iii) j_G=61.8 m/s
(b) With gas-liquid two-phase flow (j_L=0.102 m/s).

Fig.4 Visualized image of a circular-tube with a wire coil after reducing white spot noises by a morphological filter.

"Image Processing Methods to Obtain Symmetrical Distribution from Projection Image"

H. ASANO, N. TAKENAKA, T. FUJII, E. NAKAMATSU, Y. TAGAMI, K. TAKESHIMA

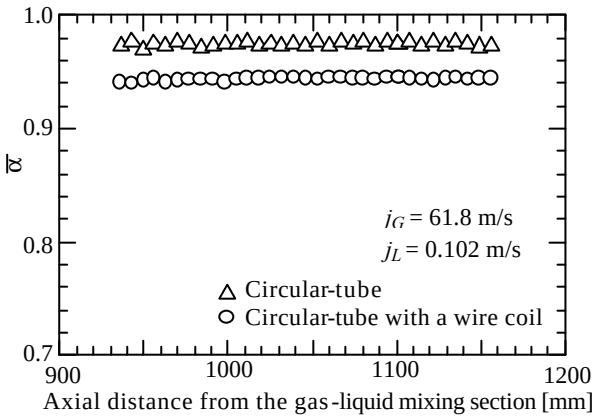

Fig. 5 Axial distribution of cross-sectional averaged void fraction.

“Image Processing Methods to Obtain Symmetrical Distribution from Projection Image”

H. ASANO, N. TAKENAKA, T. FUJII, E. NAKAMATSU, Y. TAGAMI, K. TAKESHIMA

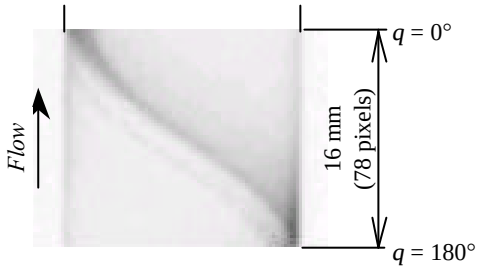

Fig. 6 Example of a sinogram.

"Image Processing Methods to Obtain Symmetrical Distribution from Projection Image"

H. ASANO, N. TAKENAKA, T. FUJII, E. NAKAMATSU, Y. TAGAMI, K. TAKESHIMA

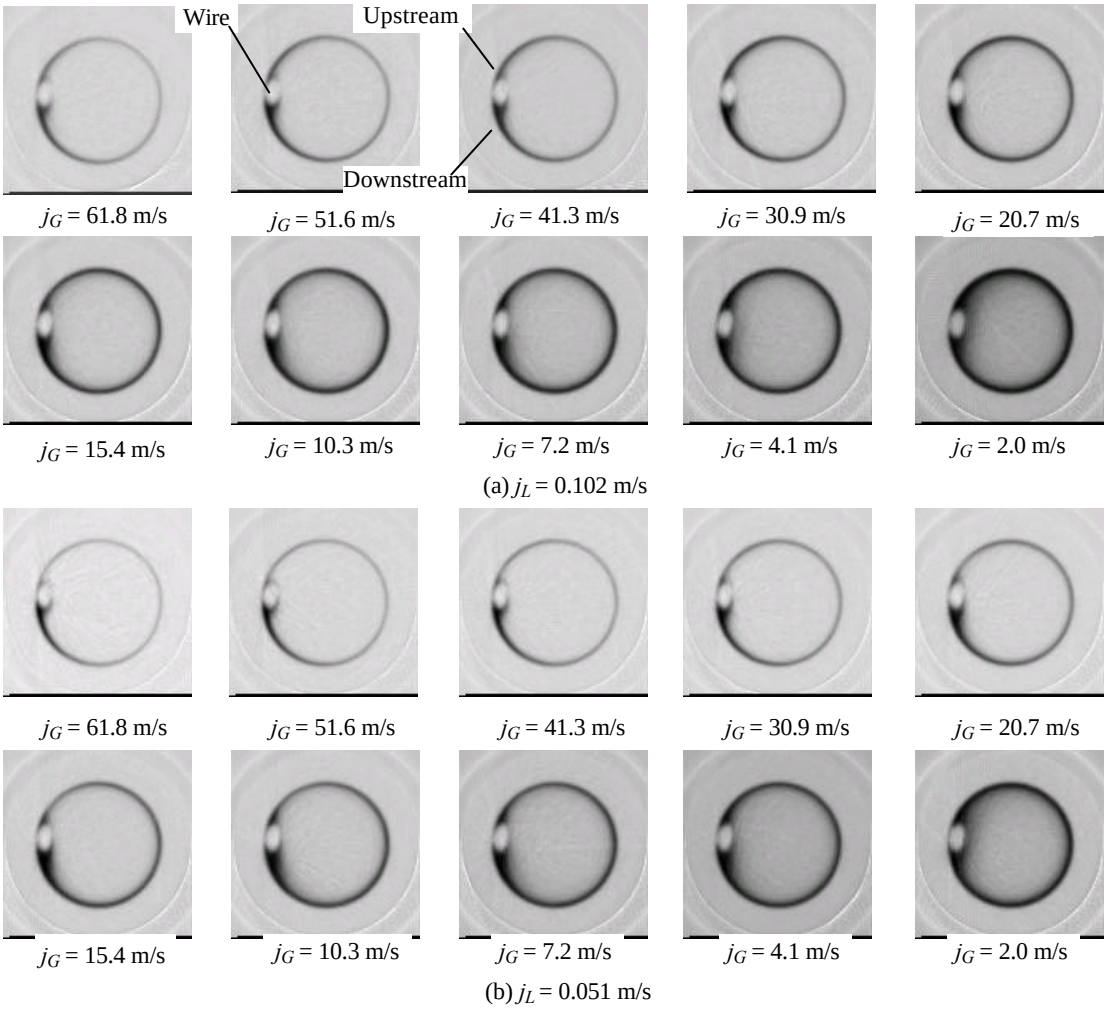

Fig.7 Cross-sectional distribution of void fraction in arbitrary unit.

"Image Processing Methods to Obtain Symmetrical Distribution from Projection Image"

H. ASANO, N. TAKENAKA, T. FUJII, E. NAKAMATSU, Y. TAGAMI, K. TAKESHIMA

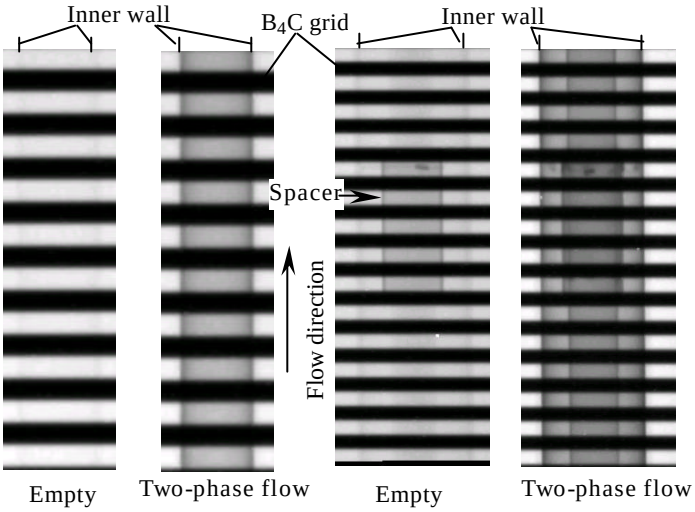

Fig.8 Visualized image after reducing white spot noises by a morphological filter.

"Image Processing Methods to Obtain Symmetrical Distribution from Projection Image"

H. ASANO, N. TAKENAKA, T. FUJII, E. NAKAMATSU, Y. TAGAMI, K. TAKESHIMA

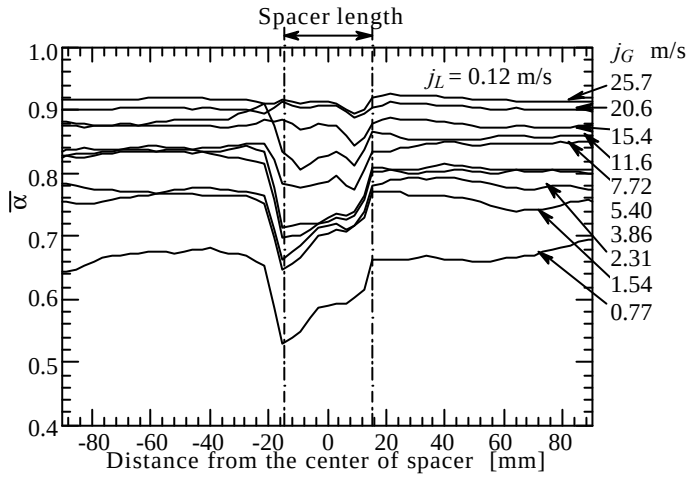

Fig.9 Axial distribution of cross-sectional averaged void fraction in a circular-tube.

“Image Processing Methods to Obtain Symmetrical Distribution from Projection Image”

H. ASANO, N. TAKENAKA, T. FUJII, E. NAKAMATSU, Y. TAGAMI, K. TAKESHIMA

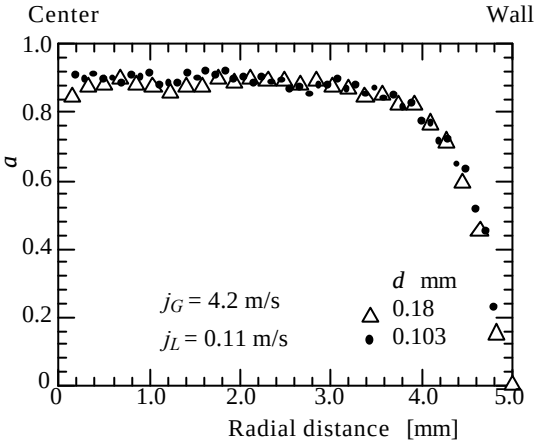

Fig. 10 Axial distribution of void fraction calculated by Abel transform (Effect of spatial resolution).

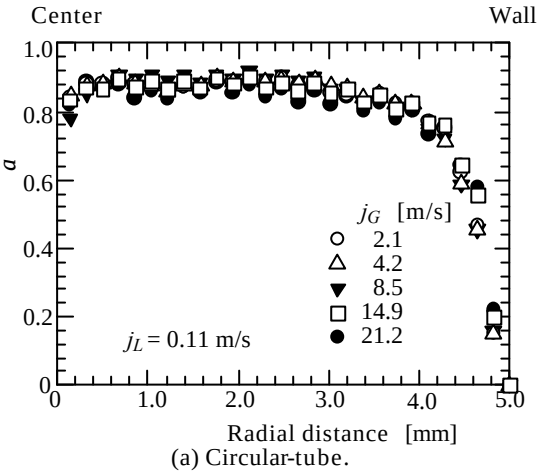

(a) Circular-tube.

Fig.11 Radial distribution of void fraction calculated by Abel transform.

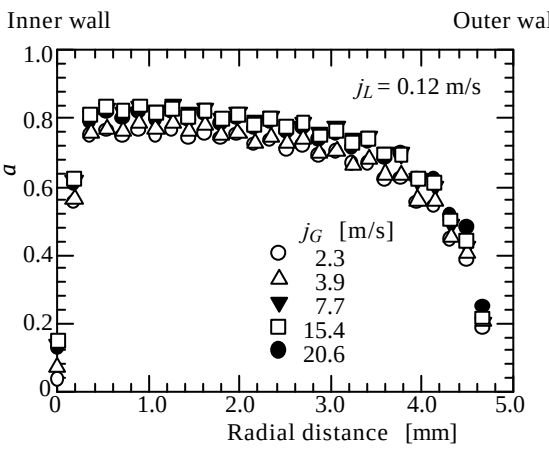

(b) Circular-tube annuli.

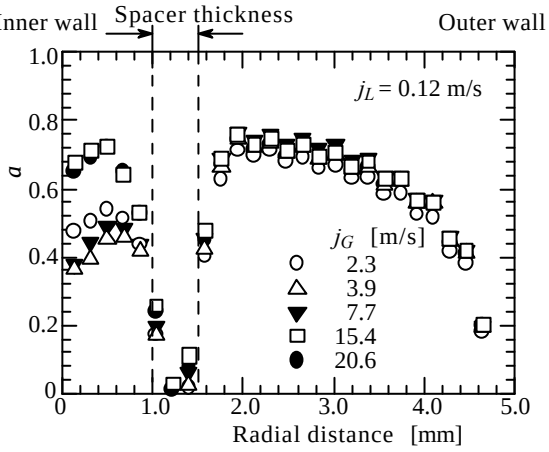

(c) Circular-tube annuli with a spacer (Center of spacer).

Fig.11 Radial distributions of void fraction calculated by Abel transform.